APS physics

CHORUS

This is the accepted manuscript made available via CHORUS. The article has been published as:

Grain-Size-Independent Plastic Flow at Ultrahigh Pressures and Strain Rates

H.-S. Park, R. E. Rudd, R. M. Cavallo, N. R. Barton, A. Arsenlis, J. L. Belof, K. J. M. Blobaum, B. S. El-dasher, J. N. Florando, C. M. Huntington, B. R. Maddox, M. J. May, C. Plechaty, S. T. Prisbrey, B. A. Remington, R. J. Wallace, C. E. Wehrenberg, M. J. Wilson, A. J. Comley, E. Giraldez, A. Nikroo, M. Farrell, G. Randall, and G. T. Gray, III

Phys. Rev. Lett. **114**, 065502 — Published 12 February 2015

DOI: 10.1103/PhysRevLett.114.065502

Grain Size Independent Plastic Flow at Ultra-high Pressures and Strain Rates

H. -S. Park* and R. E. Rudd, R. M. Cavallo, N. R. Barton, A. Arsenlis, J. L. Belof, K. J. M. Blobaum, B. S. El-dasher, J. N. Florando, C. M. Huntington, B. R. Maddox, M. J. May, C. Plechaty, S. T. Prisbrey, B. A. Remington, R. J. Wallace, C. E. Wehrenberg and M. J. Wilson
Lawrence Livermore National Laboratory, P. O. Box 808, Livermore, California 94551, USA

A. J. Comley
Atomic Weapons Establishment, Aldermaston, Reading RG7 4PR, UK

E. Giraldez, A. Nikroo, M. Farrell, G. Randall
General Atomics, 3550 General Atomics Court, San Diego, California 92121, USA

G. T. Gray III
Los Alamos National Laboratory, P. O. Box 1663, Los Alamos, New Mexico 87545, USA

(Dated: February 4, 2015)

A basic tenet of material science is that the flow stress of a metal increases as its grain size decreases, an effect described by the Hall-Petch relation. This relation is used extensively in material design to optimize the hardness, durability, survivability and ductility of structural metals. This Letter reports experimental results in a new regime of high pressures and strain rates that challenge this basic tenet of mechanical metallurgy. We report measurements of the plastic flow of the model body-centered-cubic metal tantalum made under conditions of high pressure (>100 GPa) and strain rate ($\sim 10^7$ s^{-1}) achieved using the Omega laser. Under these unique plastic deformation ("flow") conditions, the effect of grain size is found to be negligible for the grains > 0.25 μm sizes. A multiscale model of the plastic flow suggests that pressure and strain rate hardening dominate over the grain size effects. Theoretical estimates, based on grain compatibility and geometrically necessary dislocations, corroborate this conclusion.

PACS numbers: 62.20.F-, 62.50.-p, 68.35.Gy

The properties of small-grain metals are of key interest in material science [1, 2], biomaterial research [3], impact engineering [4], and space hardware designs for surviving the steady bombardment of hypervelocity interplanetary dust particles and radiation [5]. The effect of grain size on plasticity and material flow properties has been studied extensively; smaller grained materials are generally found to be stronger, at least under pressures (<10 GPa) and strain rates (<10^3 s^{-1}) [6] achievable in the laboratory using conventional techniques. An interesting open question is whether this observation, called the Hall-Petch effect, applies in high pressure (>100 GPa) and/or high strain rate ($\sim 10^7$ s^{-1}) phenomena [7, 8] such as in exoplanet formation dynamics and internal structure evolution, meteor, asteroid [9], or planetesimal impacts [10] and inertial confinement fusion implosions [11, 12]. Under these extreme conditions, material properties and plastic flow dynamics can be significantly different and difficult to predict. Theoretical uncertainties are very large, and relevant experimental data scarce to nonexistent. It was recently realized for high pressure, high strain rate conditions, that the macroscopic plastic flow stress of a material can be expressed explicitly in terms of phenomena coupled across a wide range of physical scales, including the quantum-based atomic interactions, the crystal lattice structure, dislocation mobilities on the nanoscale, and the character of the dislocation network at the mesoscale. Multiscale plasticity simulations incorporating these multiple length scales have been developed [13, 14], and differ significantly from simulations utilizing conventional models of flow stress [8], when the flow occurs at extreme pressures and strain rates. These new theoretical results offer the potential to tie the experimental observables directly to fundamental properties of the crystal and its lattice dynamics, and need to be experimentally tested and verified.

Measuring plastic deformation under dynamic loading conditions is very challenging. Diamond anvil cells (DAC) [15] attain high pressures (100-200 GPa) but at low strain rates. Gas guns, split Hopkinson bars, and

Z-pinch techniques [16] achieve higher rates, but at moderate pressures. The shock induced by irradiating a sample with a high-energy laser pulse can rapidly drive the sample to very high pressures but melts or vaporizes the sample in the process, destroying its crystalline structure. Recently, an elegant ramp compression technique has been developed [17, 18] that uses laser-generated plasma flows, instead of direct laser irradiation, to ramp-compress the samples to pressures of several hundred GPa without melting (See Figures 1 and 2). We use this platform here to experimentally examine the hihg pressure and high strain rate limit of the Hall-Petch law [19] and other models of flow stress and plasticity over a wide range of grain size, D.

The Hall-Petch law states that the yield stress or flow stress (i.e. resistance to plastic deformation) of a material varies with its grain size according to $\sigma \sim \sigma_0 + kD^{-1/2}$, where σ is the flow stress, D is the average grain diameter, and σ_0 and k are material-dependent constants [19]. The inverse square root variation of flow stress with grain size has been experimentally observed in many materials at lower pressures and strain rates, but never tested at high pressures and strain rates. Analytic constitutive models of flow stress, such as the Zerilli-Armstrong model, account for the grain size dependence by adding a $kD^{-1/2}$ term to the flow stress equation [20]. Molecular dynamics (MD) simulations of nano-crystalline fcc copper have been done with grain sizes up to tens of nm. Atomistic modeling has suggested very high flow stress under dynamic conditions in the ultra-fine grained limit at pressures below ∼100 GPa [21, 22]. There have been no dynamic experiments to test these predictions so far.

In order to measure dynamic plasticity and infer flow stress under high pressure, high strain rate conditions, we use the Rayleigh-Taylor (RT) instabilities [23, 24] to generate controlled plastic deformation, as illustrated in Fig. 1. A Ta sample is accelerated by a planar high pressure ramped pressure drive created by the high-power lasers. The resulting RT-induced plastic flow is very sensitive to average flow stress; the greater the flow stress, the lower the amount of plastic flow (Fig. 1, right hand side.) This technique of using RT instability to drive solid-state plastic flow as a measure of flow stress was first used at lower pressures with a high explosives generated drive [25]. Figure 1 shows a schematic of the experimental configuration at the Omega laser facility [26]. The applied pressure versus time ("drive") on the sample was created by focusing 40 laser beams at 351 nm wavelength and 1 ns square pulse (at a total laser energy of ∼20 kJ) into a 7 mm long, 4 mm diameter cylindrical Au radiation cavity, hohlraum, generating soft x-ray blackbody radiation at a radiation temperature of T_r ∼110 eV. The 2 mm planar experimental package is comprised of a plastic "drive reservoir", a gap, the sample to be studied, and a tamper. The rippled Ta sample also has a ∼10 μm CH_2 "heat shield" to insulate the Ta from the hot stagnating reservoir plasma. This package is attached over a hole in the side of the hohlraum, exposing the drive reservoir to x-ray radiation from the hohlraum interior. The drive reservoir consisted of a beryllium ablator facing the radiation, backed by a layer of 12.5% bromine doped CH plastic. The x-ray radiation ablates the beryllium foil, driving a strong shock through the CH(Br) reservoir which upon breakout from the back surface releases plasma across the gap, which then 'gently' stagnates onto the sample, ramping up the applied pressure over time.

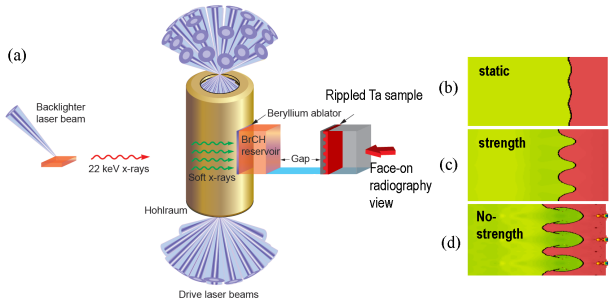

FIG. 1. (a) Schematic of the experimental setup to infer Ta material flow stress at high pressure and high strain rate at the Omega laser facility, using the Rayleigh-Taylor instability. Radiation from the hohlraum drives the reservoir/gap configuration (not to scale) creating a ramped plasma drive that compresses and accelerates the sample material without shock melting. The right panel images are 2D hydrodynamic simulations of RT-induced ripple growth; b) initial static ripples; c)with strength by the Livermore multiscale model; d) without strength . The amount of ripple growth is used to infer dynamic flow stress of the sample: the greater the flow stress, the lower the amount of ripple growth (plastic flow).

The characteristics of the pressure ramp were determined in separate laser shots using a line VISAR (velocity interferometer system for any reflector) diagnostic. The VISAR measured the particle velocity on the back surface of a thin Ta witness plate. We observed a smooth rise in particle velocity to ∼3.2 km/s over a ∼7 ns interval, corresponding to ∼130 GPa peak pressure, as shown in Figure 2 (a), a compression ratio of ρ/ρ_0 ∼1.4, and an average strain rate of $\sim 10^7$ s^{-1}. The main RT growth comes from the peak pressure where most of the acceleration happens. By matching these results with a radiation hydrodynamics simulation, we are able to infer the releasing reservoir plasma density, velocity, and temperature profiles just prior to impacting the sample [27, 28]. The evolution of the simulated sample temperature and the corresponding melting temperature as the pressure in the Ta increases are shown in Figure 2 (b) showing that our Ta sample stays below the melting temperature with a margin of a factor of ∼5.

The ripple growth is experimentally determined by face-on, in-flight, point projection radiography using a 22 keV x-ray pulse created by directing an axillary, high-intensity, short pulse laser [29] onto a silver foil

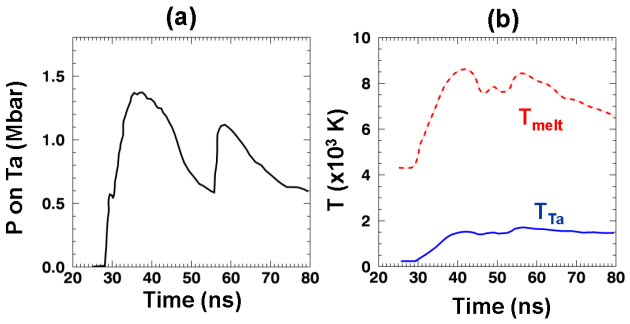

FIG. 2. (a) The simulated pressure history on the Ta target sample using a ramped plasma drive; (b) Simulated sample temperature history indicates that the sample stays well below the melting temperature during our experiment.

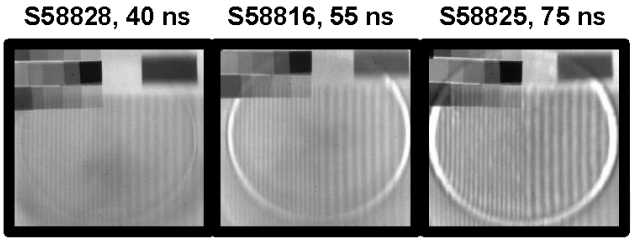

FIG. 3. Examples of face-on radiography of RT-induced ripple growth in the Ta sample at 40, 55 and 75 ns after the start of the drive laser.

located outside the hohlraum and opposite the experimental package. Examples of raw face-on radiographs at 40, 55, and 75 ns delay times are shown in Figure 3. The RT instability causes ripple "bubbles" of low density reservoir and CH_2 heat shield fluid to penetrate into the Ta increasing the contrast between the peaks and valleys as they develop in time. For each image we define a growth factor (the factor by which the rippled amplitude has increased while driven), GF, as: $GF = (\rho\Delta Z)_{driven}/\{(\rho_0\Delta Z_0)_{undriven})MTF\}$, where, ρ_0 and ΔZ_0 are the initial pre-shot density and ripple amplitude, $\rho\Delta Z$ is the measured areal density determined from the radiograph, and MTF is the modulation transfer function which quantifies the backlighter diagnostic spatial resolution. The areal density and the MTF are calibrated with in-situ step filters and Au knife-edge targets which are visible at the top of each radiograph. The error on the experimental GF is ±18%.

The bcc (body-centered-cubic) Ta samples had substrate thicknesses between 30 to 60 μm, with ripple wavelengths of 50, 100 and 150 μm and ripple amplitudes of 2.0 to 2.5 μm. The polycrystalline samples were fabricated with three different average grain sizes, 0.25±0.19, 16±6 and 92±57 μm. The smallest grain sized sample was made by sputtering and the others by wrought processing [30]. We also tested [100] and [111] single

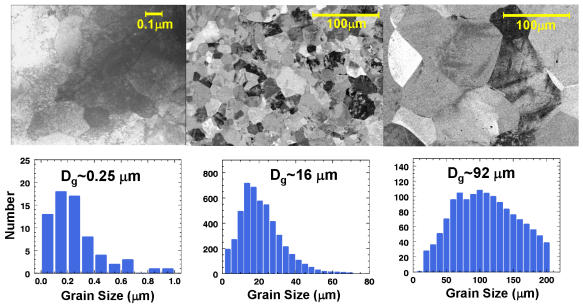

FIG. 4. Electron microscope plan view images of the Ta samples used for this experiment: sputtered sample (left); work hardened small-grain sample (middle); work hardened large-grain sample (right). The average grain sizes were 0.25±0.19 μm, 15.8±6.4 μm and 92±57 μm, respectively.

crystal Ta samples. The ripple pattern was imprinted on the surface by coining using a diamond-turned machined dye. The samples were characterized with Electron Backscatter Diffraction (EBSD), chemical analysis, electron microscopy, and indentation methods. Figure 4 shows electron microscopy images of the three samples in plan view; grain size distributions from EBSD are also shown. The grains are predominantly oriented as [111] in the out-of-plane direction. The hardnesses of the three Ta samples were determined by averaging over multiple 1 um deep Berkovich indentations in the flat region outside the coined ripple pattern, giving for the sputtered, small-grained, and large-grained samples 3.96 ± 0.25 GPa, 3.12 ± 0.18 GPa, and 2.04 ± 0.16 GPa, respectively. As expected at static ambient conditions, the samples with smaller grain size show markedly higher hardness (roughly flow stress after 8-10% plastic strain), consistent with the Hall-Petch effect.

More than 30 laser shots were taken at different ripple wavelengths, backlighter delay times, Ta sample thicknesses, and Ta grain sizes. The resulting measured GFs as a function of the delay times are shown in Figure 5. To account for variations in target sample thickness, drive laser energy, backlighter delay, and ripple wavelength, we plot GF versus the quantity $(s/\lambda)^{1/2}$, where λ is the ripple wavelength, and s the distance-traveled. The quantity $(s/\lambda)^{1/2}$ is proportional to the classical RT GF in the linear regime [31]. The 2-D ARES hydrodynamics simulation [32] was then used to predict the ripple GFs shown in the plot assuming various models of flow stress. The conventional constitutive models of Preston-Tonks-Wallace (PTW) [33], Steinberg-Guinan (SG) [34] and Steinberg-Lund (SL) [35] are seen to under-predict the Ta flow stress at these pressures and strain rates whereas the predictions of the Livermore Multiscale Strength (LMS) model [13, 14] match the data well. The LMS model connects atomistic level behavior to the continuum level plastic flow by linking density functional theory, molecular dynamics, dislocation dynamics and continuum simu-

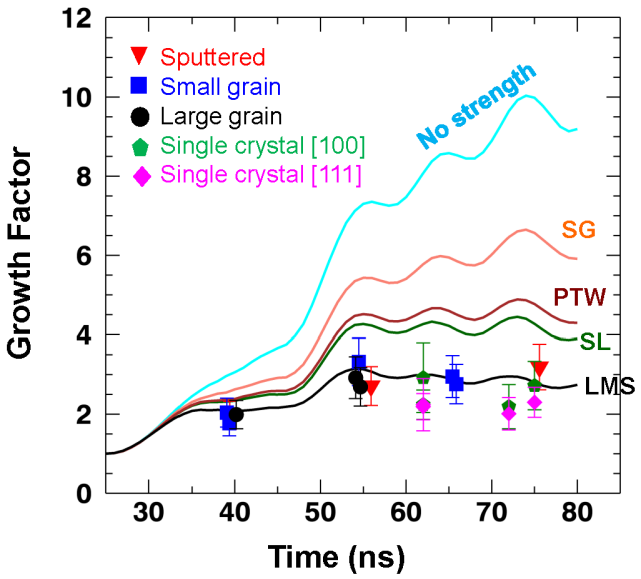

FIG. 5. Measured GF (points) compared with 2D simulations using different flow stress models referenced in the text (curves). The Livermore Multiscale Model (LMS) agrees well with the data.

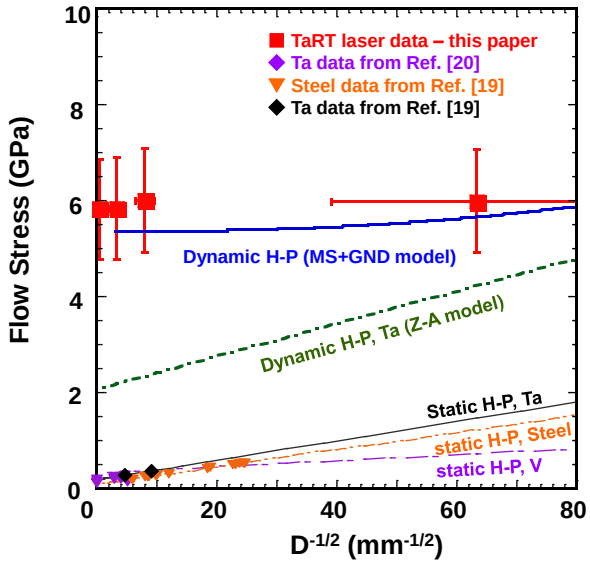

FIG. 6. Flow stress vs. $D^{-1/2}$, where D is the average grain size. The Red-square points are data from this experiment; the other points are static measurements by others. The static Hall-Petch (H-P) curves were calculated using the coefficients from [19] for Ta (solid-black), steel (dot-dot-dash-orange), and vanadium (dot-dash-purple). The dot-dash-green line is a dynamic Hall-Petch curve calculated with the Zerilli-Armstrong model assuming representative values of $P, T, \epsilon, and\ \dot{\epsilon}$. Our data show that the grain size effect is small at high-pressure and high-strain rate conditions.

lations to model flow stress as a function of P, T, ϵ, and $\dot{\epsilon}$. The LMS model gives a peak average flow stress ~6 GPa (von Mises stress) at these pressures and strain rates, which is a factor of ~8 higher than the Ta ambient flow stress of 0.8 GPa.

Our GF measurements are converted to flow stress by the LMS simulation results that match our measured GF values. Figure 6 shows the resulting flow stress values plotted against $D^{-1/2}$ along with other experimental data for Ta, steel and vanadium from conventional low pressure experiments and static Hall-Petch curves based on literature values of the Hall-Petch coefficients [19]. Also plotted (green dot-dash curve) is the prediction of the Zerilli-Armstrong (Z-A) mode;, where we added pressure hardening (via scaling with the shear modulus) [20] and the grain size contribution as an additive, rate-independent term assuming representative values of P, T, ϵ, and $\dot{\epsilon}$. The ZA model underpredicts the strength by a factor of 2.5 for the larger grain samples. This discrepancy is partially due to the model undepredicting the strain rate hardening. When we add 3000 MPa beyond the ZA model, we find that our data are marginally consistent with the H-P effect within the error bars, although a grain size-independent strength is in better agreement. Our data and simulations show that the pressure and strain rate hardening dominate over the grain size effect at these high pressures and strain rates.

To understand this lack of sensitivity of flow stress to grain size at high pressures and high strain rates, we turn to a microscopic analysis of the plastic flow. While the Hall-Petch effect in yield stress is often explained in terms of grain boundary resistance and dislocation pile-ups, the Hall-Petch effect in flow stress has been explained in terms of the generation of additional dislocation density to maintain compatibility in polycrystals during plastic deformation [19]. To calculate the effect of grain size in a simple model, we assume that grains oriented differently deform differently under stress while maintaining grain compatibility. Geometrically necessary dislocations (GND) form as a result of plastic deformations at the grain boundaries to prevent the grains from overlapping or separating to form a crack [36]. The GND-based addition to the dislocation density, ρ_{GND}, adds to the strain rate dependent dislocation density, ρ_{LMS}, in the Taylor hardening term of the LMS model of flow stress: $\sigma \approx Gb\sqrt{\rho_{LMS} + \rho_{GND}}$, where G is the shear modulus, and b the Burgers vector. For these high rate conditions, we can approximate the LMS dislocation density as the saturation density, ρ_{sat}, so the Taylor hardening term becomes $\sigma \approx Gb\sqrt{\rho_{sat} + \rho_{GND}}$. We now compare the magnitudes of ρ_{sat} and ρ_{GND}. The ρ_{sat} can be expressed as $\approx \rho_{s0}\dot{\epsilon}^n$ where ρ_{s0} is the initial dislocation density, $\dot{\epsilon}$ is the strain rate and n is 0.59 for Ta [13, 14]. The ρ_{GND} can be expressed as $\approx \epsilon/(4bD)$, where ϵ is the plastic strain, and b is Burgers vector, and D is the grain size. Taking representative values of ϵ= 0.25, b=2.86 Å, P ~100 GPa and $\dot{\epsilon} \sim 10^7$ s^{-1},

we find $\rho_{GND}(\approx (2.2\times10^{10}cm^{-2})/D(\mu m)) < \rho_{sat}(\approx 1.5\times10^{11}cm^{-2})$ showing that the GND contribution to dislocation density coming from polycrystalline compatibility is only $\sim 15\%/D$ (with D in μm) of the grain-size independent dislocation density. Hence the flow stress increase from the GND dislocation densities is small for the samples that we studied. The resulting flow stress after taking into account the GND dislocation density term is plotted in Figure 6 as the solid blue curve indicating that the grain-size dependence is small compared to the rate-dominated, grain-size independent, part of the flow stress. Our results suggest that the strain rates would need to be lower or the grain sizes would have to be <100 nm to generate observable effects in our experiments. For such small grain sizes, different mechanisms might emerge, such as grain rotation in the inverse Hall-Petch regime [2, 37].

In summary we have developed a novel laser-driven ramp compression RT technique to determine the effect of grain size on material flow stress in Ta at ∼130 GPa and $\sim 10^7$ s^{-1} peak average pressure and strain rates. Under these conditions of high pressure and high strain rate, that there is no significant flow stress difference in samples with grain sizes ranging from 0.25 to 92 μm, despite the fact that grain size has an observed $D^{-1/2}$ contribution to flow stress in conventional hardness tests at ambient conditions. We conclude that the inferred flow stress is mainly due to work hardening, strain-rate hardening, and pressure hardening, with the grain size effects being too small to be observed experimentally at these pressures and strain rates.

This work was performed under the auspices of the U.S. Department of Energy by Lawrence Livermore National Laboratory under Contract No. DE-AC52-07NA27344.

* park1@llnl.gov

[1] M. A. Meyers, A. Mishra, and D. J. Benson, Prog. Mater. Sci. **51**, 427 (2006).

[2] E. M. Bringa, A. Caro, Y. Wang, M. Victoria, J. M. McNaney, B. A. Remington, R. F. Smith, B. R. Torralva, and H. van Swygenhoven, Science **309**, 1838 (2005).

[3] M. A. Meyers, P. Y. Chen, M. I. Lopez, Y. Seki, and A. Y. M. Lin, J. Mechanical Behavior of Biomedical Materials **4**, 626 (2011).

[4] W. Walters, W. Gooch, and M. Burkins, Int. J. Impact Eng. **26**, 823 (2001).

[5] G. A. Graham, N. McBride, A. T. Kersley, G. Drolshagen, S. F. Green, J. A. M. McDonnell, M. M. Grady, and I. P. Wright, Int. J. Impact Eng. **26**, 263 (2001).

[6] D. Jia, K. T. Ramesh, and E. Ma, Acta Mater. **51**, 3495 (2003).

[7] R. E. Rudd, T. C. Germann, B. A. Remington, and J. S. Wark, MRS Bulletin **35**, 210 (2010).

[8] B. A. Remington, P. Allen, E. M. Bringa, J. Hawreliak, D. Ho, K. T. Lorenz, H. Lorenzana, J. M. McNaney, M. A. Meyers, S. W. Pollaine, K. Rosolankova, B. Sadik, M. S. Schneider, D. Swift, J. Wark, and B. Yaakobi, Mater. Sci. Tech. **22**, 474 (2006).

[9] V. V. Shuvalov and N. A. Artemieva, Planetary Space Sci. **50**, 181 (2002).

[10] R. G. Kraus *et al.*, "Shock thermodynamics of iron and impact vaporization of planetesimal cores," (2014), Nature Geoscience (submitted).

[11] J. Nuckolls, L. Wood, A. Thiessen, and G. Zimmerman, Nature **239**, 139 (1972).

[12] J. S. Ross *et al.*, "High-density carbon capsule experiments on the national ignition campaign," (2014), Phys. Rev. Lett. (submitted).

[13] N. R. Barton, J. V. Bernier, R. Becker, A. Arsenlis, R. Cavallo, J. Marian, M. Rhee, H. S. Park, B. A. Remington, and R. T. Olson, J. Appl. Phys. **109**, 073501 (2011).

[14] N. R. Barton and M. Rhee, J. of Appl. Phys. **114**, 123507 (2013).

[15] S. T. Weir, J. Akella, C. Ruddle, T. Goodwin, and L. Hsiung, Phys. Rev. B **58**, 11258 (1998).

[16] J. R. Asay, T. Ao, T. J. Vogler, J.-P. Davis, and G. T. Gray, III, J. Appl. Phys. **106**, 073515 (2009).

[17] J. Edwards, K. T. Lorenz, B. A. Remington, S. Pollaine, J. Colvin, D. Braun, B. F. Lasinski, D. Reisman, J. M. McNaney, J. A. Greenough, R. Wallace, H. Louis, and D. Kalantar, Phys. Rev. Lett. **92**, 075002 (2004).

[18] H.-S. Park, K. T. Lorenz, R. M. Cavallo, S. M. Pollaine, S. T. Prisbrey, R. E. Rudd, R. C. Becker, J. V. Bernier, and B. A. Remington, Phys. Rev. Lett. **104**, 135504 (2010).

[19] M. A. Meyers and K. K. Chawla, *Mechanical Metallurgy: Principles and Applications* (Prentice-Hall, Englewood Cliffs, New Jersey, 1984) Chap. 14.

[20] F. J. Zerilli and R. W. Armstrong, J. Appl. Phys. **68**, 1580 (1990).

[21] E. M. Bringa, K. Rosolankova, R. E. Rudd, B. A. Remington, J. S. Wark, M. Duchaineau, D. H. Kalantar, J. Hawreliak, and J. Belak, Nature Mater. **5**, 805 (2006).

[22] R. E. Rudd, Mater. Sci. Forum **633–634**, 3 (2009).

[23] L. Rayleigh, Phil. Mag. **34**, 145 (1892).

[24] G. Taylor, Proc. R. Soc. Lond. A. **201**, 192 (1950).

[25] J. F. Barnes, P. J. Blewett, R. G. McQueen, K. A. Meyer, and D. Venable, J. of Appl. Phys. **45**, 727 (1974).

[26] T. R. Boehly, R. S. Craxton, T. H. Hinterman, J. H. Kelly, T. J. Kessler, S. A. Kumpan, S. A. Letzring, R. L. McCrory, S. F. B. Morse, W. Seka, S. Skupsky, J. M. Soures, and C. P. Verdon, Review of Scientific Instruments **66** (1995).

[27] S. T. Prisbrey, H.-S. Park, B. A. Remington, R. Cavallo, M. May, S. M. Pollaine, R. Rudd, B. Maddox, A. Comley, L. Fried, K. Blobaum, R. Wallace, M. Wilson, D. Swift, J. Satcher, D. Kalantar, T. Perry, E. Giraldez, M. Farrell, and A. Nikroo, Phys. Plasmas **19**, 056311 (2012).

[28] H.-S. Park, B. A. Remington, R. C. Becker, J. V. Bernier, R. M. Cavallo, K. T. Lorenz, S. M. Pollaine, S. T. Prisbrey, R. E. Rudd, and N. R. Barton, Phys. Plasmas **17**, 056314 (2010).

[29] H. S. Park, B. R. Maddox, E. Giraldez, S. P. Hatchett, L. T. Hudson, I. N., M. H. Key, S. Le Pape, A. J. MacKinnon, A. G. MacPhee, P. K. Patel, T. W. Phillips, B. A. Remington, J. F. Seely, R. Tommasini, R. Town, J. Workman, and E. Brambrink, Phys. Plasmas **15**,

072705 (2008).
[30] S. Chen and G. Gray, Metallurgical and Materials Transactions A **27**, 2994 (1996).
[31] D. Sharp, Physica D: Nonlinear Phenomena **12**, 3 (1984).
[32] R. M. Darlington, T. L. McAbee, and G. Rodrigue, Computer Physics Communications **135**, 58 (2001).
[33] D. L. Preston, D. L. Tonks, and D. C. Wallace, J. Appl. Phys. **93**, 211 (2003).
[34] D. J. Steinberg, S. G. Cochran, and M. W. Guinan, J. Appl. Phys. **51**, 1498 (1980).
[35] D. J. Steinberg and C. M. Lund, J. Appl. Phys. **65**, 1528 (1989).
[36] M. F. Ashby, Philos. Mag. **21**, 399 (1970).
[37] J. Schiøtz, F. D. Di Tolla, and K. W. Jacobsen, Nature **391**, 561 (1998).